Pickering-Emulsion-Polymerized Polystyrene/Fe2O3 Composite Particles and Their Magnetoresponsive Characteristics

ARTICLE *in* LANGMUIR · MARCH 2013

Impact Factor: 4.46 · DOI: 10.1021/la400523w · Source: PubMed

4 AUTHORS, INCLUDING:

Ying Dan Liu
Yan Shan University
63 PUBLICATIONS **939** CITATIONS

SEE PROFILE

Hyoung Jin Choi
Inha University
392 PUBLICATIONS **7,399** CITATIONS

SEE PROFILE

Langmuir

Article

pubs.acs.org/Langmuir

Pickering-Emulsion-Polymerized Polystyrene/Fe_2O_3 Composite Particles and Their Magnetoresponsive Characteristics

Young Jae Kim,[†] Ying Dan Liu,[†,‡] Yongsok Seo,[§] and Hyoung Jin Choi*[,†]

[†]Department of Polymer Science and Engineering, Inha University, Incheon 402-751, Korea

[‡]State Key Laboratory of Metastable Materials Science and Technology, Yanshan University, Qinhuangdao 066004, People's Republic of China

[§]Intellectual Textile System Research Center (ITRC) and RIAM School of Materials Science and Engineering, Seoul National University, Seoul 151-747, Korea

ABSTRACT: Core−shell-structured magnetic polystyrene (PS)/inorganic particles were fabricated by Pickering emulsion polymerization using nanosized Fe_2O_3 particles as a solid stabilizer. Scanning electron microscopy and transmission electron microscopy confirmed the synthesized PS/Fe_2O_3 particles to be comprised of a PS surface coated with Fe_2O_3 nanoparticles. The chemical structure of the composite nanospheres was characterized by Fourier transform infrared spectroscopy and X-ray diffraction. The thermal properties of composite nanospheres and corresponding pure polymer were examined by thermogravimetric analysis. The rheological properties of the core−shell-structured magnetic PS/inorganic particles dispersed in silicone oil were investigated under an external magnetic field strength using a rotational rheometer. The particles with extremely lower density than common magnetic particles exhibited solid-like magnetorheological phase characteristics, and the flow curves were fitted to the Cho−Choi−Jhon model of the rheological equation of state.

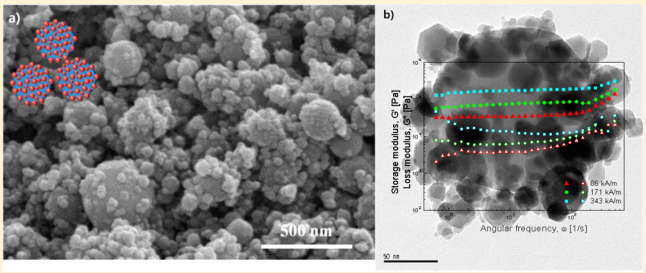

INTRODUCTION

The applications of magnetic particles have been extended to solid-dispersed substances of magnetorheological (MR) fluids, in which the MR fluids are dispersions of magnetic particles in non-magnetic medium fluids. These fluids exhibit a reversible phase change between a liquid-like and solid-like state with an external magnetic field.[1−5] Therefore, they have been applied in engineering areas, such as engine mounts, clutches, brakes, valves, and shock absorbers in the automobile industry, on account of their controllable, reversible, and improved mechanical properties and polishing characteristics.[6−9]

Among the range of magnetic particles available, the most popular MR material is the carbonyl iron (CI) particle. On the other hand, the high density of CI particles, which causes serious sedimentation problems, has limited their extensive engineering applications.[10−12] Therefore, it is important to improve this density mismatch and sedimentation problem. One potential solution, coating the CI particles, was developed using polymeric or inorganic materials and was also applicable to the fabrication of electroresponsive electrorheological particles.[13,14] Magnetic nanoparticles of different types of iron oxides [mostly maghemite (Fe_2O_3) and magnetite (Fe_3O_4)] have been used as MR materials. In particular, Fe_2O_3 nanoparticles have attracted considerable interest because of their technological and fundamental importance, such as information storage, magnetic resonance imaging contrast agent, etc.[15] In comparison to the CI particles coated using a complicated process of modifying CI particles, Fe_2O_3 particles have a much lower density than CI particles but exhibit significant magnetic behavior.[16,17]

Inorganic/organic core−shell-structured particles constructed by the Pickering emulsion process have recently been introduced. In this method, the solid inorganic particles are used as a surfactant instead of conventional molecular organic surfactants.[18] Nanometer-sized particles are adsorbed at the oil−water interface for stabilization because of the decrease in interfacial energy after replacing a part of the liquid−liquid or liquid−vapor interface with a liquid−solid particle interface. A range of Pickering emulsions has attracted increasing interest for practical applications in the development of novel nano- and microstructures,[19−23] in which the solid particles used in Pickering emulsions can vary from latex particles, inorganic particles, semiconductor nanoparticles, to polymer micelles.[24−26] Pickering emulsions stabilized by magnetic nanoparticles have also been reported.[27−32] Recently, Yin et al. fabricated a magnetite-coated polystyrene (PS) microsphere using Pickering emulsion polymerization and studied its catalytic property.[33]

In this study, Fe_2O_3-coated polystyrene (PS/Fe_2O_3) particles were synthesized using 50 nm diameter spherical Fe_2O_3 nanoparticles as a stabilizer, and their MR properties were examined at various magnetic field strengths when dispersed in

Received: February 7, 2013
Revised: March 26, 2013
Published: March 27, 2013

silicone oil. The incorporation of the polymer core and the Fe_2O_3 shell not only reduced the density of the magnetic particles but also improved the dispersibility of the Fe_2O_3 nanoparticles. The morphology of the particles obtained was found to be different from that of the commonly used CI-based composite MR particles because they are not only a core−shell-structured material but also a Fe_2O_3 shell possessing a magnetoresponsive MR effect rather than a PS core.

EXPERIMENTAL SECTION

Materials. Styrene (density of 0.9 g/cm^3; Daejung, Korea) and 2,2′-azobis(2-methyl-propionamidine) dihydrochloride (AIBA) (97%; Sigma-Aldrich) were used as a monomer and cationic water-soluble initiator, respectively. Fe_2O_3 nanoparticles (density, 5.12 g/cm^3; particle size, <50 nm) were purchased from Sigma-Aldrich.

Synthesis of PS/Fe_2O_3 Particles. The PS/Fe_2O_3 composite particles were synthesized by Pickering emulsion polymerization[34,35] using Fe_2O_3 nanoparticles as a stabilizer. To 200 mL of deionized water, 5 g [~50% (v/v) to the monomer] of Fe_2O_3 nanoparticles were added and then ultrasonicated for 30 min. Herein, the amount of Fe_2O_3 nanoparticle was determined by several times attempt. After ultrasonication, 9 g [5% (v/v) to the aqueous phase] of the styrene monomer was added to the Fe_2O_3 dispersion and agitated vigorously in a homogenizer until the styrene layer was well-dispersed in the aqueous phase as emulsified droplets. The resulting emulsion was poured into a 250 mL round-bottomed three-neck flask, which was then sealed with a rubber seal and bubbled with nitrogen for 30 min. An aqueous AIBA solution (0.1 g of AIBA/5 mL of deionized water) was then added, and the system was heated to 65 °C. The reaction was kept for 12 h at 65 °C, and the final product was then washed with both methanol and distilled water to remove the excess initiator, monomer, and free Fe_2O_3 nanoparticles and dried in a freeze dryer for 3 days.

To prepare the MR fluid, the dried composite particles were dispersed in silicone oil (kinematic viscosity of 10 cSt) with a particulate volume fraction of 25% (46.7% in weight) and sonicated for 1 h to obtain a uniformly dispersed MR fluid. As a comparable MR fluid sample, pristine Fe_2O_3 nanoparticles were dispersed in silicone oil with the same volume fraction.

Characterization. The morphology of the synthesized PS/Fe_2O_3 particles was observed by scanning electron microscopy (SEM, S-4300 Hitach) and transmission electron microscopy (TEM, Philips CM200). The chemical structure of the product was characterized by Fourier transform infrared spectroscopy (FTIR, Perkin-Elmer System 2000). The crystal structures of the samples were examined by X-ray diffraction (XRD, DMAX-2500, Rigaku). The degree of the polymer-coating amount was measured by thermogravimetric analysis (TGA, TA Instruments Q50, New Castle, DE) at a heating rate of 10 °C/min in nitrogen gas with a temperature range of 25−800 °C. A vibrating sample magnetometer (VSM, DMS 1660) was used to examine the magnetic characteristics over a broad magnetic field range. The MR behavior of the synthesized particle-based MR fluid was confirmed using a rotational rheometer (MCR 300, Physica, Stuttgart, Germany) equipped with a MR device (MCR 180), which generates a homogeneous magnetic field.

RESULTS AND DISCUSSION

Figure 1 shows SEM and TEM images of the surface morphology of the PS/Fe_2O_3 composite particles, in which spherical PS/Fe_2O_3 particles (150−300 nm) exhibited an uneven surface. Note that, through Pickering emulsion polymerization, styrene droplets were stabilized by Fe_2O_3 nanoparticles dispersed in deionized water. As a stabilizer, Fe_2O_3 nanoparticles were positioned at the interface of the styrene droplets to stabilize the oil/water (O/W) system. Polymerization occurred immediately after adding the AIBA while keeping the Fe_2O_3 nanoparticles adsorbed at the surface

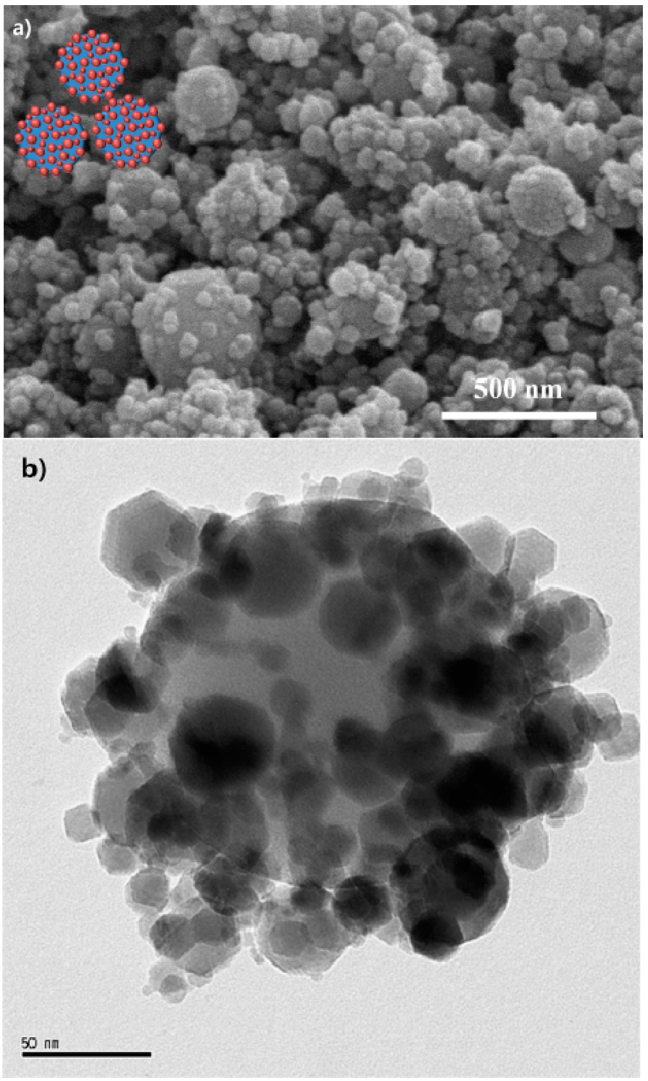

Figure 1. SEM (a) and TEM (b) images of PS/Fe_2O_3 particles.

of the PS particles. SEM (Figure 1a) of the PS/Fe_2O_3 particles shows that the bumpy surface of the PS particles is due to the attached Fe_2O_3 nanoparticles, which act as a stabilizer during Pickering emulsion polymerization. In addition to PS/Fe_2O_3 particles synthesized, free Fe_2O_3 particles could also be observed from the SEM image, implying that the amount of Fe_2O_3 nanoparticles added to the Pickering emulsion system is higher than needed. Note that SEM of PS particles from either emulsion[36] or dispersion[37] polymerization can be compared. TEM of the core−shell-structured PS particles in Figure 1b clearly shows that the larger spheres are PS cores and surrounding particles are Fe_2O_3 nanoparticles, confirming the structure of the PS/Fe_2O_3 particles and the Pickering emulsion of Fe_2O_3 nanoparticles as a stabilizer. The size of the PS/Fe_2O_3 particles observed by TEM is similar to that by SEM.

FTIR spectroscopy measurement (Figure 2) was performed to examine the chemical structures of the Fe_2O_3, PS, and PS/Fe_2O_3 particles, in which each particle was loaded in KBr pellets and scanned over the wavenumber ranging from 4000 to 400 cm^{-1}, before which a baseline was scanned in a vacuum environment at room temperature. The broad band with a low intensity at 3400 cm^{-1} reveals the presence of hydroxyl groups on the ferric oxide surface. Bands at approximately 561 cm^{-1}

dx.doi.org/10.1021/la400523w | Langmuir 2013, 29, 4959−4965

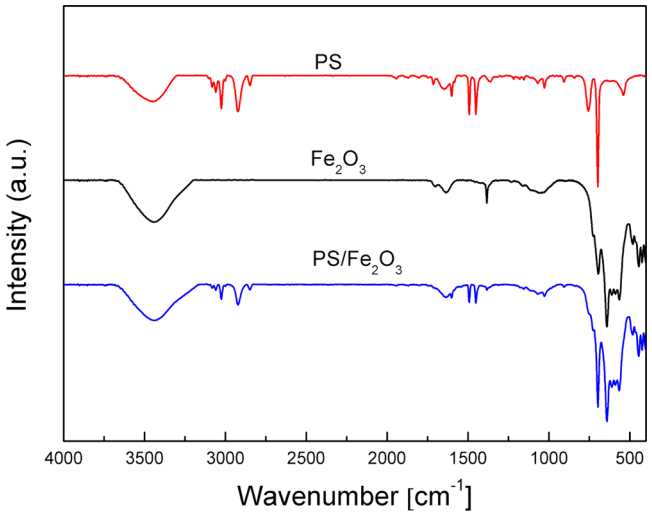

Figure 2. FTIR spectra of pure Fe_2O_3, PS, and PS/Fe_2O_3 particles.

are assigned to Fe−O vibration modes. From the FTIR spectrum of PS, peaks for the aromatic ring stretching vibrations are observed at 1600−1430 cm^{-1}. The bands near 760 and 690 cm^{-1} confirm the presence of a monosubstituted aromatic group. In addition, the C−H stretching vibration is detected at 2975−2950 cm^{-1}. The FTIR spectrum of the PS/Fe_2O_3 particles exhibits the typical chemical characteristics of both PS and Fe_2O_3 nanoparticles.

Figure 3 shows the thermal decomposition behavior of the PS, Fe_2O_3, and PS/Fe_2O_3 particles determined by TGA. The

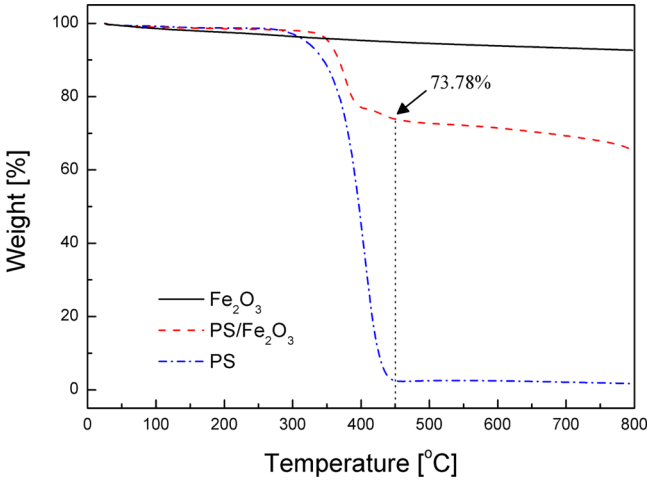

Figure 3. TGA spectrum of pure Fe_2O_3, PS, and synthesized PS/Fe_2O_3 particles.

decomposition temperature of the PS/Fe_2O_3 composite particles is obviously higher than that of the corresponding pure PS. This improvement in the thermal stability of the PS/Fe_2O_3 particles is attributed to the protective effect of the Fe_2O_3 shell, which restricts thermal motion of the PS chains and helps prevent the degradation of PS particles. According to TGA, the weight percentage of Fe_2O_3 and PS in the PS/Fe_2O_3 particles is 73.78 and 26.22%, respectively. The density of the Fe_2O_3 and PS particles is 5.12 and 1.09 g/cm^3, respectively. In contrast, the calculated density of PS/Fe_2O_3 was 2.60 g/cm^3, which is much lower than that of pure Fe_2O_3 particles. The density of 2.46 g/cm^3 measured using a gas pyconometer is lower than the density obtained from TGA. This suggests that the composite particle volume increases because of the impurities absorbed on the PS/Fe_2O_3 particle surface because of its magnetic properties.

Figure 4 shows the magnetic hysteresis loops measured in the powder state for pure Fe_2O_3 and PS/Fe_2O_3 particles. The

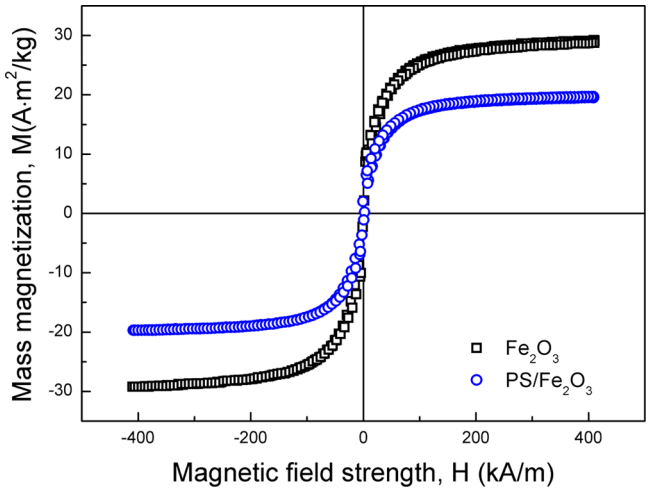

Figure 4. VSM data of pure Fe_2O_3 and PS/Fe_2O_3 particles.

saturation magnetization (Ms) of the particles was reduced from 30 to 20 A m^2 kg^{-1} because of the introduction of an organic PS core. The reduction of the Ms (10/30 = 33.33%) is higher than the weight percentage (26.22%, w/w) of PS particles in the composite. Thereby, it can be considered that the incorporation of PS particles not only enlarges the total mass of the particles but also weakens the direct interaction of the magnetic particles. Therefore, a MR suspension based on PS/Fe_2O_3 particles will show weak MR performance compared to that of pure Fe_2O_3 particles because the saturation magnetization of magnetic particles is an important factor influencing the MR effect.

XRD of PS, rare Fe_2O_3, and PS/Fe_2O_3 particles was performed to identify the crystal structure of the Fe_2O_3 particles (Figure 5). The XRD patterns of the rare Fe_2O_3

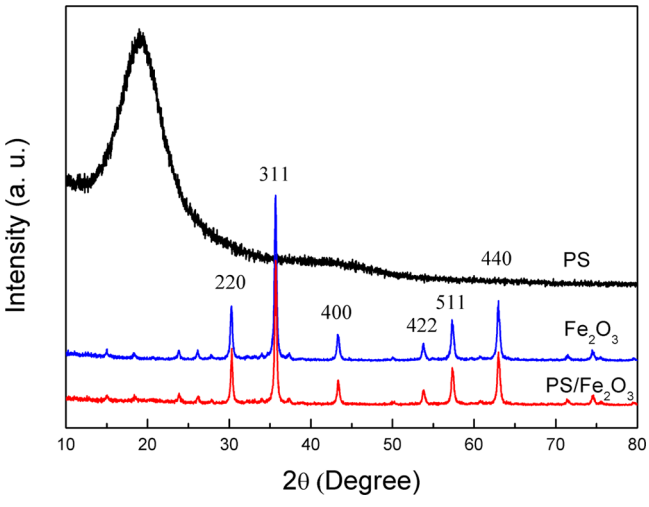

Figure 5. XRD patterns of pure PS, pure Fe_2O_3, and synthesized PS/Fe_2O_3 particles.

dx.doi.org/10.1021/la400523w | Langmuir 2013, 29, 4959−4965

particles and Fe_2O_3-coated PS spheres show similar characteristic peaks for Fe_2O_3 particles at 2θ of 30.2, 35.6, 43.3, 53.7, 57.3, and 62.9°.[28] The peak intensities of rare Fe_2O_3 with synthesized PS/Fe_2O_3 are similar. This is because the Fe_2O_3 nanoparticles are located at the surface of the PS cores after polymerization according to the mechanism of Pickering emulsion polymerization.

Two MR fluids with the same volume percentage of 25% were prepared on the basis of pure Fe_2O_3 and PS/Fe_2O_3 particles. The shear rate sweep test was operated at a shear rate ranging from 0.01 to 900/s on a log−log scale under different magnetic field strengths. As shown in Figures 6 and 7, both MR fluids exhibit a step increase in shear stress and shear viscosity with an increasing magnetic field strength. The MR fluid of rare Fe_2O_3 particles shows relatively higher shear stress as well as higher shear viscosity than that shown by the PS/Fe_2O_3-based MR fluid. With the same particulate volume fraction, the MR fluid of pure Fe_2O_3 possesses more magnetic part than the MR fluid of PS/Fe_2O_3 composites, thus giving higher Ms, as shown in Figure 4. It is just like replacing a part of Fe_2O_3 particles by non-magnetic PS, which will reduce the magnetic interactions between the particles. Note that MR fluids with a higher Ms of magnetic particles always demonstrate higher MR characteristics.[13] Without a magnetic field, the PS/Fe_2O_3-based MR fluid exhibited typical non-Newtonian behavior, in which the shear stress increased linearly with an increasing shear rate in the log−log plot with a slope of about 0.5, which is deviated from 1.0 of Newtonian fluid behavior (Figure 6). Meanwhile, the rare Fe_2O_3-based MR fluid showed a steep increase in shear stress when no magnetic field was applied. This might be caused by the poor dispersion state of the inorganic Fe_2O_3 nanoparticles in silicone oil. Although a magnetic field was applied, the shear stress curves of the Fe_2O_3 MR fluid were different from the plateau behavior over the entire range of applied shear rates for the pure CI microbead system.[38] In the low shear rate region on the applied magnetic fields, the shear stress curves showed a dented line shape with a critical shear rate point. The shear stress increased rapidly after the critical shear rate region. This behavior is similar to the phenomenon observed for an electrorheological (ER) fluid under an applied electric field.[39] This is not the same as the PS/Fe_2O_3 MR fluid, which suggests lower but more stable shear stress over the entire shear rate range. The formation of this aggregate has been suggested to be driven by lowering the free energy in the system because of particle−particle interactions.[40] With the applied magnetic fields, it is well-known that chain-like structures of the dispersed magnetic particles formed spontaneously.[6] Chain formation via optical microscopy can be found for either MR elastomer[41,42] or ER fluid.[43] The structures of the particles were broken and rearranged with an increase in the shear rate. At the critical shear rate point, the rate of destruction of the chain-like structures became faster than the reforming rate by the magnetic field. Finally, the shear stress curve was similar to the flow curves without a magnetic field applied.

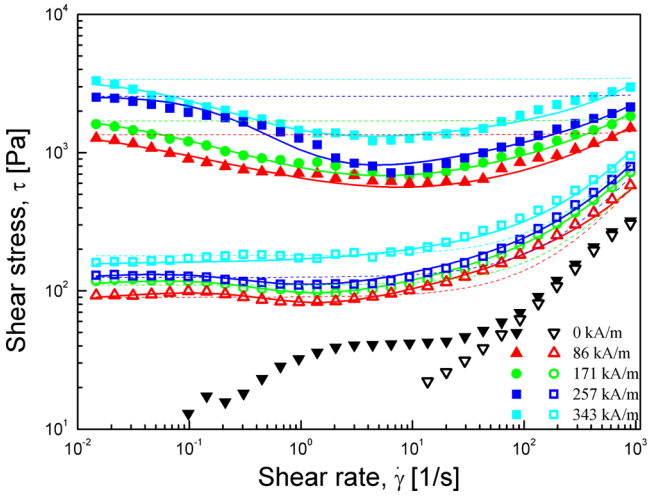

Figure 6. Shear stress versus shear rate of pure Fe_2O_3 (closed symbols) and PS/Fe_2O_3 (open symbols) MR fluids at various magnetic field strengths. The dotted and solid lines are generated from the Bingham and CCJ models with an optimal parameter, respectively.

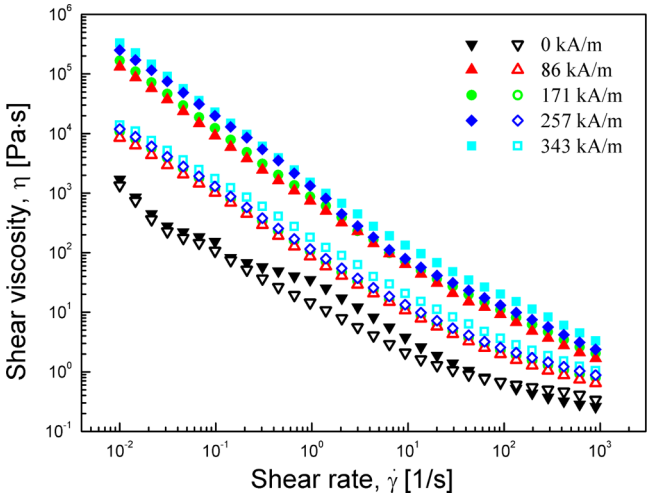

Figure 7. Shear viscosity versus shear rate of pure Fe_2O_3 (closed symbols) and PS/Fe_2O_3 (open symbols) MR fluid at various magnetic field strengths.

The Bingham fluid model was used to fit the shear rate−shear stress curve with the parameters derived from the yield stress τ_o and Newtonian viscosity η_o. On the other hand, this model was unable to fit the flow curves in Figure 6 over the entire shear rate range. Therefore, another model was adopted, the Cho−Choi−Jhon (CCJ) model,[44] in terms of six parameters, which are described as follows:

$$\tau = \frac{\tau_0}{1 + (t_2\dot{\gamma})^{\alpha}} + \eta_\infty\left(1 + \frac{1}{(t_3\dot{\gamma})^{\beta}}\right)\dot{\gamma} \quad (1)$$

where τ_0 is the yield stress defined as the extrapolated stress at the low shear rate region and η_∞ is the viscosity at a high shear rate and is interpreted as the viscosity in the absence of a magnetic field. The exponents, α and β, are related to the increase and decrease in shear stress. t_2 and t_3 on the right-hand side of the equation are the time constants that can adjust the fitting curves in the low and high shear rate regions, respectively. Table 1 lists the optimal parameters.

The dynamic yield stresses obtained from the flow curves at various magnetic field strengths were plotted as a function of the magnetic field strength on a log−log scale (Figure 8). In general, the dependency of the dynamic yield stress on the magnetic field strength can be represented by the following power law relationship:

dx.doi.org/10.1021/la400523w | Langmuir 2013, 29, 4959−4965

Table 1. Fitting Parameters of Bingham and CCJ Model Equations to the Flow Curves of Pure Fe_2O_3 and PS/Fe_2O_3 Particle-Based MR Fluid

		magnetic field strength (kA/m)			
model	parameter	1.0	2.0	3.0	4.0
		Pure Fe_2O_3			
Bingham	τ	1350	1700	2550	3400
	η	0.1	0.1	0.1	0.1
CCJ	τ	1800	2000	2300	3000
	t_2	14	10	3.3	8
	α	0.4	0.55	1.1	0.8
	η_∞	0.49	0.6	0.72	1.25
	t_3	0.00035	0.00037	0.0004	0.0006
	β	0.75	0.8	0.85	0.9
		PS/Fe_2O_3			
Bingham	τ	90	110	125	180
	η	0.5	0.5	0.6	0.8
CCJ	τ	60	75	80	85
	t_2	2	2.5	3	4
	α	1.3	1.2	1.1	0.5
	η_∞	0.35	0.56	0.63	0.8
	t_3	0.0017	0.0029	0.00297	0.003
	β	0.82	0.84	0.857	0.89

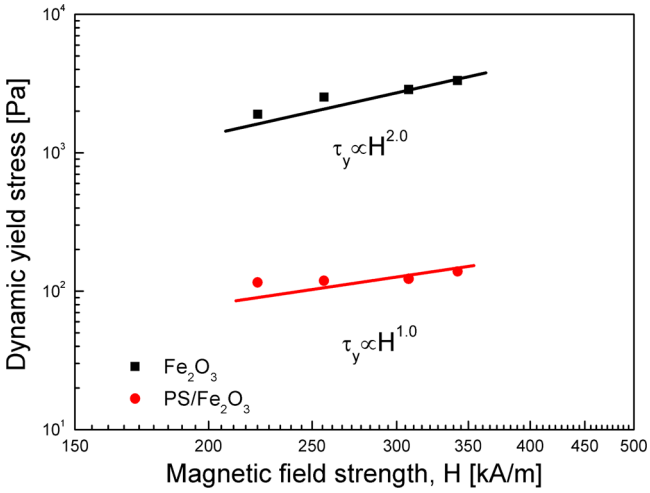

Figure 8. Fitting parameters of the Bingham and CCJ model equations to the flow curves of the pure Fe_2O_3 and PS/Fe_2O_3 particle-based MR fluid.

$$\tau_y \propto H^m \tag{2}$$

The yield stress is approximately proportional to the magnetic field strength, where the slope of the single line is 2.0 in the linear magnetization regime, i.e., $\tau_y \propto H^2$ corresponding to the magnetic polarization model based on magnetiztatic interactions.[45] An analogy between electrostatic and magnetostatic interactions in the linear region for the polarization model has been investigated for both ER[46] and MR fluids, respectively. The Fe_2O_3-based MR fluid followed the magnetic polarization model correctly. The same relationship was also shown by a ferrofluid based on magnetite nanoparticles for both dynamic and static yield stresses.[42] On the other hand, the exponent parameter becomes 1.0 for the PS/Fe_2O_3-based MR fluid. This is different from the classic polarization model because the MR properties are affected by the mass magnetization and connection probability of the particles. The Fe_2O_3 nanoparticles were coated on the surface of the PS core disproportionately, as observed by SEM and TEM. In addition, the PS/Fe_2O_3 particles exhibited magnetic properties from surface to surface only and not from the PS cores. These can affect the field dependence of the MR properties of the MR fluids. It can also be noted that the slope of 1.0 has been observed for giant ER fluids, in which the polar molecules adsorbed on the particles are considered to be the driving force, making their aggregation into columns aligned along the field direction. Thus, the yield stress of giant ER fluid exhibits a nearly linear dependence upon the applied electric field.[47,48]

An oscillatory test was also carried out under different magnetic field strengths to determine the viscoelastic properties of MR fluids, before which the demagnetization process was carried out to eliminate the effect of the residual magnetic property remaining in the particles. Figure 9 shows the

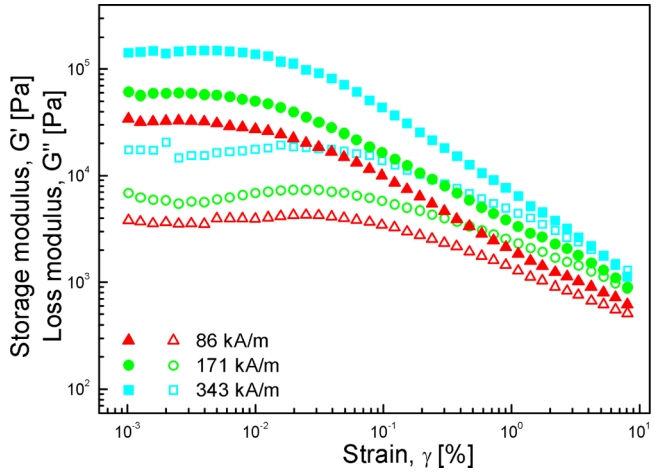

Figure 9. Amplitude sweep for the PS/Fe_2O_3 MR fluid under a range of magnetic field strengths. Storage modulus, G' (closed symbols); loss modulus, G'' (open symbols).

amplitude sweep measurements describing the changes in the storage modulus (G') and loss modulus (G'') as a function of the strain amplitude for the MR fluids, in which G' and G'' represent the elasticity and viscous behavior, respectively. The amplitude sweep experiment was performed at a constant angular frequency of 6.28 rad/s in various strains of 0.001−10%. The constant angular frequency was determined in the amplitude sweep, which was suggested by the test system. Figure 9 shows that G' is much higher than G'' at the applied magnetic field. This suggests that the MR fluids are more solid-like rather than liquid-like under an applied magnetic field. A strain amplitude of 0.002% was selected in the plateau regime of G' and applied to perform the frequency sweep.

Figure 10 shows the dynamic moduli (G' and G'') of the MR fluids, which were measured over the angular frequency range of 0.1−600 rad/s. The values of G' were higher than G'', indicating that the elastic behaviors are dominant over viscous behaviors in the structure of a MR fluid.[7,49] On the other hand, the whole particulate chains over the two plates of the geometry were not strong enough to be sustained under high frequencies because both G' and G'' increase slightly with frequency. However, under an applied magnetic field, there is a possibility such that those broken chains reform structure again, as also shown in Figure 6. Similarly, in the case of ER fluid, the fibrillation of ER particles in shear flow is reported to be a

dx.doi.org/10.1021/la400523w | Langmuir 2013, 29, 4959−4965

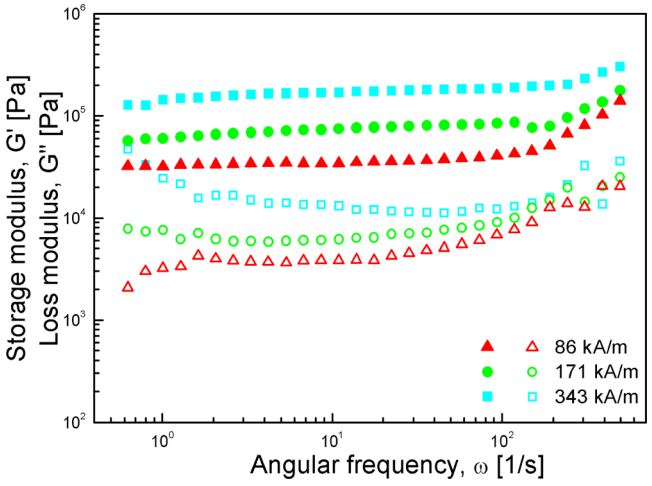

Figure 10. Frequency sweep for a PS/Fe_2O_3 MR fluid under a range of magnetic field strengths. Storage modulus, G' (closed symbols); loss modulus, G'' (open symbols).

breaking and reformation process caused by the cooperation of electrostatic and hydrodynamic interactions, which are reduced by an external electric and flow field.[42] This explanation could be extended to the MR fluid under an oscillatory shear in this study. This phenomenon weakens when the magnetic field strength becomes higher; i.e., both G' and G'' showed plateau behavior over the entire frequency range when the magnetic field strength was higher than 171 kA/m. Stronger particle chains were formed under a higher magnetic field strength. On the other hand, it can also be noted that, in comparison to the MR fluid based on ferrofluid recently reported,[42] in which the crossover from viscous behavior to elastic behavior occurs at a crossover frequency, where stresses in the system relax within a finite time, no crossover frequency was observed.

CONCLUSION

Magnetic PS/Fe_2O_3 particles were synthesized using the Pickering emulsion method. SEM and TEM showed that the PS core particles were coated with Fe_2O_3 nanoparticles. XRD verified the accurate crystalline structure of the synthesized PS/Fe_2O_3 particles. The VSM graph indicated that mass magnetization decreased from 30 A m^2 kg^{-1} for pure Fe_2O_3 to 20 A m^2 kg^{-1} for Ps/Fe_2O_3 particles. A MR fluid based on the PS/Fe_2O_3 particles experienced rotational and oscillatory measurements at an applied magnetic field. The flow curve was fitted to the CCJ model, and the yield stress of PS/Fe_2O_3 was rearranged to a straight line to understand the relationship between the magnetic strength and yield stress. Although MR characterization exhibited lower shear stress than the pure Fe_2O_3-based MR fluid, typical MR behavior was well-preserved in both the shear and oscillatory tests.

AUTHOR INFORMATION

Corresponding Author

*E-mail: hjchoi@inha.ac.kr.

Notes

The authors declare no competing financial interest.

ACKNOWLEDGMENTS

This study was supported by research funding from Hyundai Automobile (2012).

REFERENCES

(1) Santiago-Quinonez, D. I.; Rinaldi, C. Enhanced rheological properties of dilute suspensions of magnetic nanoparticles in a concentrated amphiphilic surfactant solution. *Soft Matter* **2012**, *8*, 5327−5333.
(2) Lopez-Lopez, M. T.; Gomez-Ramirez, A.; Rodriguez-Arco, L.; Duran, J. D. G.; Iskakova, L.; Zubarey, A. Colloids on the frontier of ferrofluids. Rheological properties. *Langmuir* **2012**, *28*, 6232−6245.
(3) Ramos, J.; Klingenberg, D. J.; Hidalgo-Alvarez, R.; de Vicente, J. Steady shear magnetorheology of inverse ferrofluids. *J. Rheol.* **2011**, *55*, 127−152.
(4) Tian, Y.; Jiang, J.; Meng, Y.; Wen, S. A shear thickening phenomenon in magnetic field controlled-dipolar suspensions. *Appl. Phys. Lett.* **2010**, *97*, 151904.
(5) Yamaguchi, H.; Niu, X. D.; Ye, X. J.; Li, M.; Iwamoto, Y. Dynamic rheological properties of viscoelastic magnetic fluids in uniform magnetic fields. *J. Magn. Magn. Mater.* **2012**, *324*, 3238−3244.
(6) de Vicente, J.; Ruiz-Lopez, J. A.; Andablo-Reyes, E.; Segovia-Gutierrez, J. P.; Hidalgo-Alvarez, R. Squeeze flow magnetorheology. *J. Rheol.* **2011**, *55*, 753−779.
(7) Claracq, J.; Sarrazin, J.; Montfort, J. P. Viscoelastic properties of magnetorheological fluids. *Rheol. Acta* **2004**, *43*, 38−49.
(8) Ido, Y.; Inagaki, T.; Yamaguchi, T. Numerical simulation of microstructure formation of suspended particles in magnetorheological fluids. *J. Phys.: Conden. Matter* **2010**, *22*, 324103.
(9) Chooi, W. W.; Oyadiji, S. O. Mathematical modeling, analysis, and design of magnetorheological (MR) dampers. *Trans. ASME* **2009**, *131*, 061002.
(10) Fang, F. F.; Choi, H. J.; Choi, W. S. Two-layer coating with polymer and carbon nanotube on magnetic carbonyl iron particle and its magnetorheology. *Colloid Polym. Sci.* **2010**, *288*, 359−363.
(11) Rich, J. P.; Doyle, P. S.; McKinley, G. H. Magnetorheology in an aging, yield stress matrix fluid. *Rheol. Acta* **2012**, *51*, 579−593.
(12) Cheng, H. B.; Wang, J. M.; Zhang, Q. J.; Wereley, N. M. Preparation of composite magnetic particles and aqueous magneto-rheological fluids. *Smart Mater. Struct.* **2009**, *18*, 085009.
(13) Fang, F. F.; Choi, H. J.; Seo, Y. Sequential coating of magnetic carbonyliron particles with polystyrene and multiwalled carbon nanotubes and its effect on their magnetorheology. *ACS Appl. Mater. Interfaces* **2010**, *2*, 54−60.
(14) Liu, Y. D.; Choi, H. J. Electrorheological fluids: Smart soft matter and characteristics. *Soft Matter* **2012**, *8*, 11961−11978.
(15) Tejada, J.; Zhang, X. X.; Balcells, L. Nonthermal viscosity in magnets—Quantum tunneling of the magnetization. *J. Appl. Phys.* **1993**, *73*, 6709−6714.
(16) Son, Y. H.; Lee, J. K.; Soong, Y.; Martello, D.; Chyu, M. Structure−property correlation in iron oxide nanoparticle−clay hybrid materials. *Chem. Mater.* **2010**, *22*, 2226−2232.
(17) Degen, P.; Wieland, D. C. F.; Leick, S.; Paulus, M.; Rehage, H.; Tolan, M. Effect of magnetic nanoparticles on the surface rheology of surfactant films at the water surface. *Soft Matter* **2011**, *7*, 7655−7662.
(18) Zhou, J.; Qiao, X.; Binks, B. P.; Sun, K.; Bai, M.; Li, Y.; Liu, Y. Magnetic Pickering emulsions stabilized by Fe_3O_4 nanoparticles. *Langmuir* **2011**, *27*, 3308−3316.
(19) Okada, M.; Maeda, H.; Fujii, S.; Nakamura, Y.; Furuzono, T. Formation of Pickering emulsions stabilized via interaction between nanoparticles dispersed in aqueous phase and polymer end groups dissolved in oil phase. *Langmuir* **2012**, *28*, 9405−9412.
(20) Schrade, A.; Mikhalevich, V.; Landfester, K.; Ziener, U. Synthesis and characterization of positively charged, alumina-coated silica/polystyrene hybrid nanoparticles via Pickering miniemulsion polymerization. *J. Polym. Sci., Part A: Polym. Chem.* **2011**, *49*, 4735−4746.
(21) Chen, W.; Liu, X.; Liu, Y.; Kim, H. I. Synthesis of microcapsules with polystyrene/ZnO hybrid shell by Pickering emulsion polymerization. *Colloid Polym. Sci.* **2010**, *288*, 1393−1399.
(22) Kim, J.; Cote, L. J.; Kim, F.; Yuan, W.; Shull, K. R.; Huang, J. X. Graphene oxide sheets at interfaces. *J. Am. Chem. Soc.* **2010**, *132*, 8180−8186.

(23) Vignati, E.; Piazza, R.; Lockhart, T. P. Pickering meulsions: Interfacial tension, colloidal layer morphology, and trapped-particle motion. *Langmuir* **2003**, *19*, 6650−6656.
(24) Gao, Q. X.; Wang, C. Y.; Liu, H. X.; Wang, C. H.; Liu, X. X.; Tong, Z. Suspension polymerization based on inverse Pickering emulsion droplets for thermo-sensitive hybrid microcapsules with tunable supracolloidal structures. *Polymer* **2009**, *50*, 2587−2594.
(25) Ma, H.; Luo, M. X.; Sanyal, S.; Rege, K.; Dai, L. L. The one-step pickering emulsion polymerization route for synthesizing organic−inorganic nanocomposite particles. *Materials* **2010**, *3*, 1186−1202.
(26) Liu, H. X.; Wang, C. Y.; Gao, Q. X.; Liu, X. X.; Tong, Z. Magnetic hydrogels with supracolloidal structures prepared by suspension polymerization stabilized by Fe_2O_3 nanoparticles. *Acta Biomater.* **2010**, *6*, 275−281.
(27) Qiao, X. Y.; Zhou, J.; Binks, B. P.; Gong, X. L.; Sun, K. Magnetorheological behavior of Pickering emulsions stabilized by surface-modified Fe_3O_4 nanoparticles. *Colloid Surf., A* **2012**, *412*, 20−28.
(28) Xiao, Q.; Tan, X. K.; Ji, L. L.; Xue, J. Preparation and characterization of polyaniline/nano-Fe_3O_4 composite via a novel Pickering emulsion route. *Synth. Met.* **2007**, *157*, 784−791.
(29) Hasell, T.; Yang, J. X.; Wang, W. X.; Li, J.; Brown, P. D.; Poliakoff, M.; Lester, E.; Howdle, S. M. Preparation of polymer−nanoparticle composite beads by a nanoparticle-stabilised suspension polymerization. *J. Mater. Chem.* **2007**, *17*, 4382−4386.
(30) Shen, S. L.; Wu, W.; Guo, K.; Meng, H.; Chen, J. F. A novel process to synthesize magnetic hollow silica microspheres. *Colloids Surf., A* **2007**, *311*, 99−105.
(31) Liu, H. X.; Wang, C. Y.; Gao, Q. X.; Chen, J. X.; Liu, X. X.; Tong, Z. One-pot fabrication of magnetic nanocomposite microcapsules. *Mater. Lett.* **2009**, *63*, 884−886.
(32) Ning, Y.; Wang, C. Y.; Ngai, T.; Yang, Y.; Tong, Z. Hollow magnetic Janus microspheres template from double Pickering emulsions. *RSC Adv.* **2012**, *2*, 5510−5512.
(33) Yin, D.; Du, X.; Liu, H.; Zhang, Q.; Ma, L. Facile one-step fabrication of polymer microspheres with high magnetism and armored inorganic particles by Pickering emulsion polymerization. *Colloids Surf., A* **2012**, *414*, 289−295.
(34) Zhang, Y.; Zou, Q.; Shu, X.; Tang, Q.; Chen, M.; Wu, L. Preparation of raspberry-like polymer/silica nanocomposite microspheres via emulsifier-free polymerization in water/acetone media. *J. Colloid Interface Sci.* **2009**, *336*, 544−550.
(35) Song, X.; Yang, Y.; Liu, J.; Zhao, H. PS colloidal particles stabilized by graphene oxide. *Langmuir* **2011**, *27*, 1186−1191.
(36) Cochin, D.; Laschewsky, A.; Nallet, F. Emulsion polymerization of styrene using conventional, polymerizable, and polymeric surfactants. A comparative study. *Macromolecules* **1997**, *30*, 2278−2287.
(37) Liu, Y. D.; Park, B. J.; Kim, Y. H.; Choi, H. J. Smart monodisperse polystyrene/polyaniline core−shell structured hybrid microspheres fabricated by a controlled releasing technique and their electro-responsive characteristics. *J. Mater. Chem.* **2011**, *21*, 17396−1702.
(38) Liu, Y. D.; Choi, H. J.; Choi, S. B. Controllable fabrication of silica encapsulated soft magnetic microspheres with enhanced oxidation−resistance and their rheology under magnetic field. *Colloid Surf., A* **2012**, *403*, 133−138.
(39) Lee, B. M.; Kim, J. E.; Fang, F. F.; Choi, H. J.; Feller, J. F. Rectangular-shaped polyaniline tubes covered with nanorods and their electrorheology. *Macromol. Chem. Phys.* **2011**, *212*, 2300−2307.
(40) Tao, R.; Sun, J. M. Three-dimensional structure of induced electrorheological solid. *Phys. Rev. Lett.* **1991**, *67*, 398.
(41) Mietta, J. L.; Ruiz, M. M.; Antonel, P. S.; Perez, O. E.; Butera, A.; Jorge, G.; Negri, R. M. Anisotropic magnetoresistance and piezoresistivity in structured Fe_3O_4−silver particles in PDMS elastomers at room temperature. *Langmuir* **2012**, *28*, 6985−6996.
(42) Felicia, L. J.; Philip, J. Probing of field-induced structures and tunable rheological properties of surfactant capped magnetically polarizable nanofluids. *Langmuir* **2013**, *29*, 110−120.
(43) Liu, Y. D.; Fang, F. F.; Choi, H. J. Core−shell structured semiconducting PMMA/polyaniline snowman-like anisotropic microparticles and their electrorheology. *Langmuir* **2010**, *26*, 12849−12854.
(44) Cho, M. S.; Choi, H. J.; Jhon, M. S. Shear stress analysis of a semiconducting polymer based electrorheological fluid system. *Polymer* **2005**, *46*, 11484−11488.
(45) Ginder, J. M.; Davis, L. C.; Elie, L. D. Rheology of magnetorheological fluids: Models and measurements. *Int. J. Mod. Phys. B* **1996**, *10*, 3293−3303.
(46) Yin, J. B.; Zhao, X. P. Preparation and enhanced electrorheological activity of TiO_2 doped with chromium ion. *Chem. Mater.* **2004**, *16*, 321−328.
(47) Lu, K. Q.; Shen, R.; Wang, X. Z.; Sun, G.; Wen, W. J.; Liu, J. X. Polar molecule dominated electrorheological effect. *Chin. Phys.* **2006**, *15*, 2476−2480.
(48) Liu, Y. D.; Choi, H. J. Electrorheological fluids: Smart soft matter and characteristics. *Soft Matter* **2012**, *8*, 11961−11978.
(49) Mantripragada, S.; Wang, X.; Gordaninejad, F.; Hu, B.; Fuchs, A. Rheological properties of novel magnetorheological fluids. *Int. J. Mod. Phys. B* **2007**, *21*, 4849−4857.